Probing the exchange bias in Co/CoO nanoscale antidot arrays using anisotropic magnetoresistance

D. Tripathy and A. O. Adeyeye*
Department of Electrical and Computer Engineering, Information Storage Materials Laboratory, National University of Singapore, Singapore 117576
(Received 28 October 2008; published 18 February 2009)

The dependence of exchange bias in polycrystalline Co/CoO nanoscale antidot arrays on temperature and Co layer thickness t_{Co} has been systematically probed using the anisotropic magnetoresistance technique. Our experimental results reveal a relatively small degree of asymmetry in the magnetization reversal process of the antidot arrays as compared to a continuous film of identical composition, attributable to the configurational anisotropy of the antidot arrays and the competition between interfacial ferromagnetic-antiferromagnetic (FM-AFM) exchange anisotropy and FM uniaxial anisotropy. The strong interplay between thermal activation effects and AFM domain size confinement in the antidot arrays results in the exchange bias field H_E being either smaller or larger than the continuous film depending on the temperature. Furthermore, with increasing t_{Co}, the asymmetry in the magnetization reversal of the antidot arrays increases monotonously due to enhancement in the FM anisotropy. This enhancement is accompanied by a reduction in the magnitudes of H_E and coercive field H_C with increasing t_{Co} at all temperatures.

DOI: 10.1103/PhysRevB.79.064413 PACS number(s): 75.75.+a, 73.43.Qt, 75.60.Jk, 75.70.Cn

I. INTRODUCTION

There has been sustained interest in the exchange bias phenomenon, which is a magnetic proximity effect that typically occurs due to interfacial exchange coupling at ferromagnetic-antiferromagnetic (FM-AFM) interfaces. This coupling could give rise to an induced unidirectional anisotropy in the FM layer, thereby leading to the displacement of the magnetic hysteresis loop along the magnetic field axis.[1–5] This shift in the hysteresis loop, or the exchange bias field H_E, is often accompanied by an enhancement in the coercive field H_C.[6–8] The exchange bias is usually established by cooling the FM-AFM system from above the Néel temperature T_N of the AFM material in the presence of an external magnetic field. By employing such a field-cooling procedure, spins at the FM-AFM interface are "frozen" in a predefined direction. Although the microscopic origin of the exchange bias effect is still not elucidated completely despite exhaustive experimental and theoretical studies,[4] it has been extensively utilized in several magnetoelectronic applications. Exchange bias has been used to pin the magnetization orientation of the FM layer, which then serves as the reference layer for key devices in magnetic sensors and high-density magnetic data storage, for instance, in spin valves and magnetic tunnel junctions.[9]

With the development of advanced lithography tools for fabricating nanostructures with controlled dimensions and geometry,[10,11] there has been a constant miniaturization in the physical dimensions of magnetic elements in recent years. As the dimensions become comparable to certain relevant length scales in magnetism (spin diffusion length, domain size, domain wall width, etc.), the properties of nanostructures differ significantly from continuous films. This has subsequently triggered extensive studies on the magnetic properties of exchange biased nanostructures.[12–24] From a fundamental point of view, investigation of exchange bias in systems with lateral dimensions comparable to AFM or FM domain sizes is crucial since it allows probing of the role of domains in exchange bias[12,14,18] and also aids in understanding the influence of lateral confinement and shape anisotropy on exchange bias fields and magnetization reversal mechanisms.[22,25] Alternately, from a technological aspect, exchange bias can be employed as a tunable source of unidirectional anisotropy to stabilize the magnetization in nanostructures and, hence, enables reduction in length scales that determine the superparamagnetic limit.[16]

In continuous FM/AFM bilayers, it has been shown that the AFM layer thickness dependence of exchange bias can be used to directly establish the effect of AFM anisotropy.[26] For extreme cases of very thin AFM layers, no exchange bias effect was observed in the system.[26,27] Similarly, the effects of varying the thickness of the AFM layer, as well as altering the lateral dimensions, have also been extensively studied in exchange biased nanostructures.[18,23,24] It has been shown that reducing the lateral dimensions of the exchange biased system results in changes in the asymmetry of the magnetization reversal mechanisms[16,19] and enhancement in the coercive field H_C.[12,14,16,18] It is important to note however that there is no universal dependence of the exchange bias field H_E on the dimensions of the nanostructures. Recently, we have demonstrated for antidot arrays, which consist of "nonmagnetic holes" or antidots embedded in a continuous exchange biased film, that H_E is larger than the continuous film at room temperature and increases progressively as the diameter of the antidots is increased.[12] While similar enhancement in H_E was also observed in other nanostructures,[16,17] a variety of exchange biased systems exhibits the opposite trend.[14,18–20,22] This discrepancy clearly illustrates the difficulty in inferring systematic trends on the magnitude of exchange bias fields and is attributable to the AFM and FM materials employed, (differing FM and AFM domain sizes and anisotropies), the nanostructure form (varying shape anisotropies), or the lithography technique employed.

In this work, we have probed in detail using anisotropic magnetoresistance (AMR), the exchange bias effect in nano-

scale Co/CoO antidot arrays as a function of temperature and FM layer thickness. We have employed the Co/CoO system due to its Néel temperature T_N (291 K), which is just below room temperature, thus enabling the exchange bias to be reset conveniently. Our results demonstrate that the asymmetry in magnetization reversal of Co/CoO bilayers is markedly modified due to the presence of antidots and is strongly dependent on the FM layer thickness. We also observe that the exchange bias field in the antidot arrays can be either larger or smaller than the continuous film, depending on the temperature. The interfacial nature of the FM-AFM coupling in the exchange biased antidot arrays is further established from the dependence of H_E and H_C on the FM layer thickness.

II. EXPERIMENTAL DETAILS

The nanoscale antidot arrays were fabricated over a large area (4×4 mm^2) on commercially available Si substrates using deep ultraviolet (DUV) lithography at 248 nm exposing wavelength. To create patterns in resist, the substrates were initially coated with 60-nm-thick antireflective layer followed by 480 nm of positive DUV photoresist, which is four to five times thicker than those used in electron beam lithography. This allows for the fabrication of antidots with high aspect ratio and also makes the lift-off process easier. A Nikon lithographic scanner with KrF excimer laser radiation was used for exposure, leading to the formation of resist dots. The antidot pitch on the mask was kept at 415 nm. To convert these resist patterns into antidots, Co(t_{Co})/CoO(5 nm)/Cu(2 nm) multilayers were subsequently deposited using *e*-beam evaporation at room temperature. The exchange biased multilayers were then removed from the unexposed areas by ultrasonic assisted liftoff in OK73 resist thinner. Lift-off completion was determined by the color contrast of the patterned film and confirmed by inspection under a scanning electron microscope (SEM). The final structure consists of exchange biased antidot arrays of diameter 265 nm and edge-to-edge spacing of 150 nm in a square lattice geometry, as shown in Fig. 1(a). Details of the fabrication process are described elsewhere.[28]

To probe the magnetotransport properties, electrical contacts were made on the exchange biased antidot arrays using standard optical lithography, followed by deposition of Cr (10 nm)/Au (200 nm) by thermal evaporation and subsequent liftoff in acetone. As shown in Fig. 1(b), the choice of contact geometry differs from that used in the standard four-probe dc technique. The standard four-probe dc technique results in nonuniform current-density distribution in the large area antidot arrays and, hence, reduced sensitivity to magnetoresistance (MR).[29] In an earlier work, it has been shown using experimental studies and finite element simulations on current-density distributions that the standard four-probe technique completely changes the sign of MR response in rectangular antidot structures due to the presence of orthogonal current flow.[30,31] To circumvent this problem, the unconventional contact geometry was used to ensure unidirectional current flow in the exchange biased antidot arrays.[32]

The MR response from the exchange biased antidot array and a continuous film deposited under identical conditions

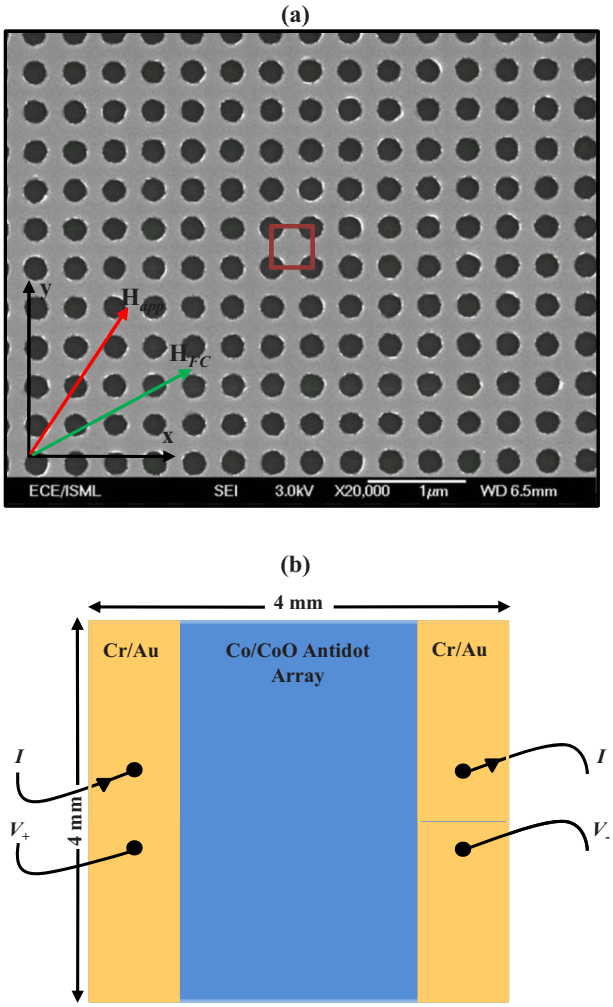

FIG. 1. (Color online) (a) Scanning electron micrograph of Co (25 nm)/CoO (5 nm)/Cu (2 nm) antidot arrays after liftoff and (b) schematic of electrical contact geometry used in the AMR measurements.

were measured simultaneously in the temperature range of $5\ \text{K}\leq T\leq 300\ \text{K}$ using a custom-designed cryogenic sample holder to ensure identical experimental conditions for both samples during measurement. The exchange bias was set by field cooling the samples in the presence of an in-plane magnetic field $H_{FC}=5$ kOe from $T=300$ K (above the Néel temperature $T_N=291$ K for bulk CoO) to the desired set point temperature T along the edge of the square lattice. Magnetic properties of the antidot arrays were characterized as a function of temperature using a vibrating sample magnetometer (VSM). The exchange bias was set in the samples using the field-cooling technique described above. After each measurement, the samples were warmed back to $T=300$ K to reset the exchange bias. As reported earlier,[33] exchange biased Co/CoO systems with thicker CoO layers ($t_{CoO}\geq5$ nm) reveal smaller training effects as compared to thinner CoO layers. Although training effects were negligible for our Co/CoO antidot arrays and films due to the choice of thicker CoO layer, we started the data acquisition only after the first five loops had been completed. The results presented in this work thus correspond to the state when no further variations in exchange bias or coercive fields occur.

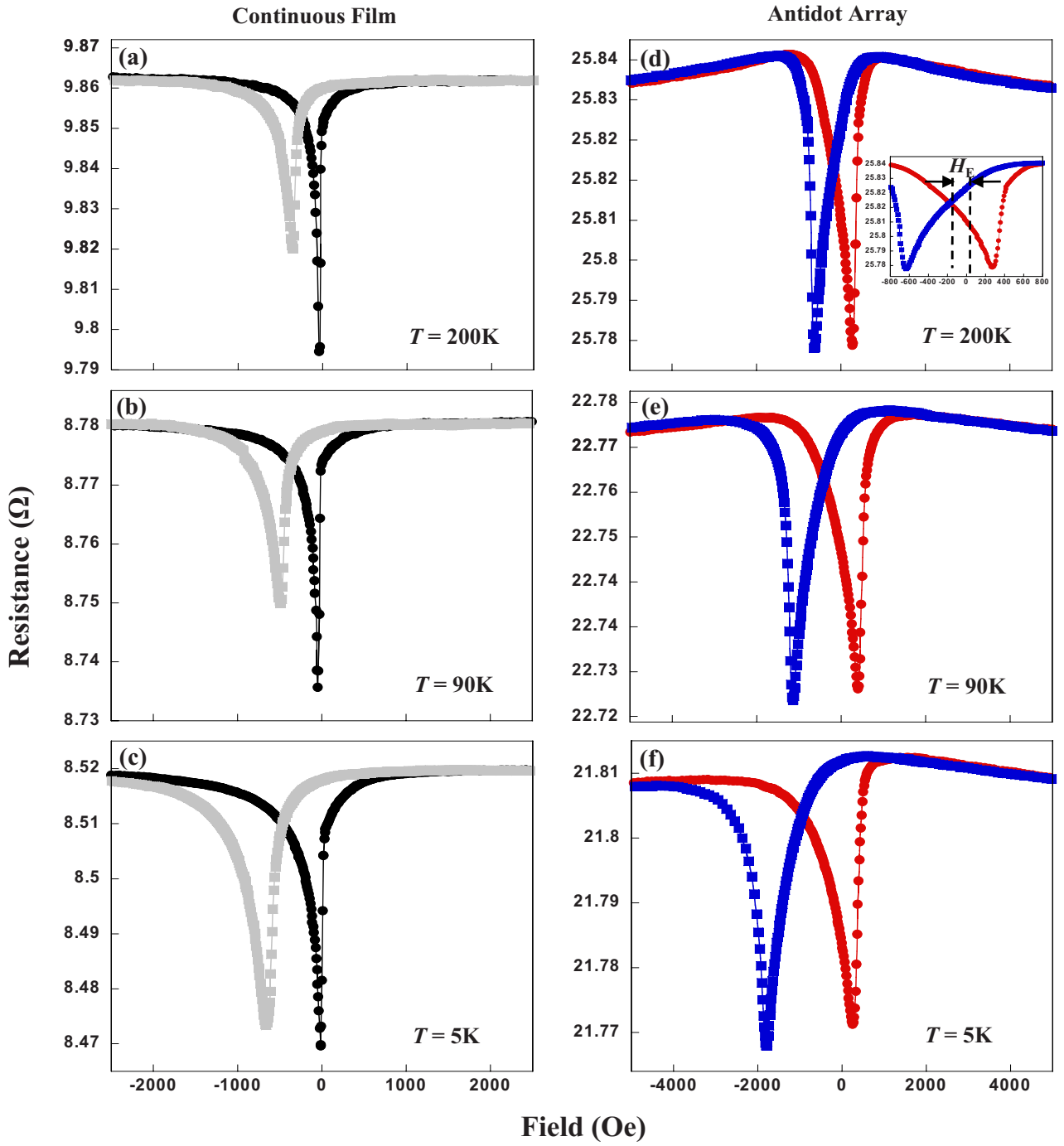

FIG. 2. (Color online) Longitudinal AMR curves as a function of temperature for the exchange biased continuous film and antidot array of composition Co (25 nm)/CoO (5 nm)/Cu (2 nm). The dots represent the sweep from negative to positive saturation field, while the squares represent the sweep from positive to negative saturation field.

III. RESULTS AND DISCUSSION

A. Comparison of magnetization reversal in antidot arrays and continuous films

The magnetization reversal in Co/CoO antidot arrays and the corresponding continuous film was systematically investigated using the AMR technique, which has been demonstrated to be a versatile tool for the investigation of exchange bias.[34] Moreover, measurement of exchange bias using AMR is much faster as compared to hysteresis loops using either VSM or superconducting quantum interference device (SQUID). The AMR effect is caused by spin-orbit scattering, and for a saturated ferromagnet, it depends on the relative orientation of current density and magnetization.[35] Figure 2 shows the representative longitudinal AMR curves for Co (25 nm)/CoO (5 nm)/Cu (2 nm) antidot arrays and the corresponding continuous film as a function of temperature. The samples were field cooled in H_{FC}=5 kOe from T=300 K

(along the edge of the square lattice for the antidot array) and also measured along the same direction. For all measurements, the magnetic field was swept parallel to the current density, along the field-cooling direction. The resistance has a maximum in both the saturated states, i.e., parallel and antiparallel to the field-cooling direction and a minimum when the magnetization is perpendicular to the field-cooling direction.

At $T=200$ K, we observed that the AMR curve for the continuous film is shifted by $H_E=257$ Oe from the zero-field axis, and the magnetization reversal is highly asymmetric as illustrated clearly by the difference in heights of the AMR peaks at both the coercive fields shown in Fig. 2(a). To obtain the degree of asymmetry, the AMR curves were normalized and the difference in heights of the AMR peaks at both coercive fields was divided by the AMR at the second coercive field (i.e., in the decreasing branch). Using the above definition, we obtain an asymmetry of 0.28% at 200 K. The asymmetric nature of the AMR curve is attributed to different reversal mechanisms dominating the increasing and decreasing branches of the curve. In the decreasing branch, the magnetization reversal is primarily due to nucleation of reversed domains and propagation of domain walls since the magnetization is mostly collinear with the field-cooling direction. In the increasing branch, however, the reversal is due to rotation of the magnetization at the coercive field. Similar asymmetry in magnetization reversal has also been addressed in other Co/CoO bilayer systems[36–39] and patterned systems.[19,40] The origin of such asymmetric reversal has been ascribed to a variety of factors such as existence of higher-order FM anisotropies,[41] dispersion of the FM or AFM anisotropy axis,[42,43] and competition between the FM uniaxial anisotropy and interfacial FM-AFM exchange anisotropy.[44] Theoretical studies employing numerical investigations of the domain state model have shown that depending on the angle between the field-cooling direction and the AFM anisotropy axis, magnetization reversal occurs either by coherent rotation for both loop branches or is asymmetric with a nonuniform reversal in the decreasing branch.[45] As the temperature is reduced, it was observed that the asymmetry in the AMR curves decreases gradually to 0.16% at 90 K and reduces further to 0.01% at 5 K. This trend in asymmetry is closely related to changes in the ratio of K_U/K_E as a function of temperature, where K_U and K_E are the uniaxial and unidirectional anisotropies.[44] The stability of the interfacial exchange coupling varies in different regions of the FM/AFM interface. In certain regions, the coupling is weak due to the presence of defects or roughness, while in other regions the coupling is comparatively stronger. Both these regions contribute to the uniaxial anisotropy K_U at all temperatures. However, it has been shown previously that the FM-AFM freezing temperature is proportional to the strength of the interfacial exchange coupling.[46,47] Hence, contributions to the unidirectional anisotropy K_E at high temperatures come predominantly from the regions of strong exchange coupling, while the regions with reduced coupling start contributing only as the temperature is reduced. Hence, the ratio K_U/K_E reduces with decreasing temperature, thereby resulting in a reduction in the asymmetry of the AMR curves. The magnetization reversal processes in the continuous film and the resulting trends in the temperature dependence of asymmetry are thus consistent with the competition between K_U and K_E.[38]

In contrast to the continuous film, we observed that the corresponding AMR curve for the antidot array exhibits a relatively small degree of asymmetry at $T=200$ K and is shifted by $H_E=175$ Oe. A discussion on the comparative magnitudes of H_E as a function of temperature for both the antidot arrays and the continuous film will be presented in Sec. III B. We observed that the coercive field for the antidot array is greatly enhanced as compared to the continuous film. This is attributed to the fact that antidots act as "pinning centers" which hinder the propagation of domain walls, thus increasing the coercivity. Another prominent characteristic that was not observed in the continuous film is a small linear increase in resistance as the external magnetic field is reduced from saturation for the antidot arrays. This behavior results from a slight misalignment between the current density and magnetization at saturation due to geometrical confinement introduced by the antidots.[32] The linear increase in resistance thus indicates that the local spins are more aligned with the current density during the initial reduction in external magnetic field from saturation. Moreover, since the thickness of the Co/CoO bilayers and the dimensions of the antidot arrays are both in the nanometer regime, the formation of domain walls is likely to be impeded in the antidot arrays.[48] Hence, magnetization reversal in the antidot arrays is most likely realized by spin rotation rather than domain wall motion. The relatively small asymmetry in the AMR curves may be attributed to the highly ordered geometry of the antidot arrays. We have shown earlier that due to configurational anisotropy, antidot arrays with square lattice geometry exhibit biaxial anisotropy with an easy axis along the diagonal direction and hard axes along the edges of the square unit cell in order to minimize the magnetostatic energy.[49] The observed periodicity in the anisotropy is due to geometrical equivalence as the antidot array is rotated every 90°. For FM/AFM bilayers, it has been shown that the asymmetry in magnetization reversal is observed only for a range of angles from the easy axis, the magnitude of which is determined by the competition between FM uniaxial anisotropy and the interfacial FM-AFM exchange anisotropy.[44] Since the AMR curves for the antidot arrays were measured with magnetic field applied along the edge of the square lattice (corresponding to the hard axis and hence beyond the range of angles for exhibiting large asymmetry), in agreement with the above argument, the asymmetry between the reversals in the increasing and decreasing branches of the curve is extremely small. It was also observed that unlike the continuous film, variations in the degree of asymmetry for the antidot arrays are minimal as the temperature is reduced.

B. Temperature dependence of exchange bias and coercive fields

The evolution in exchange bias field H_E has been systematically studied as a function of temperature to emphasize the importance of thermal activation effects in exchange biased nanostructures, especially in light of some of the conflicting

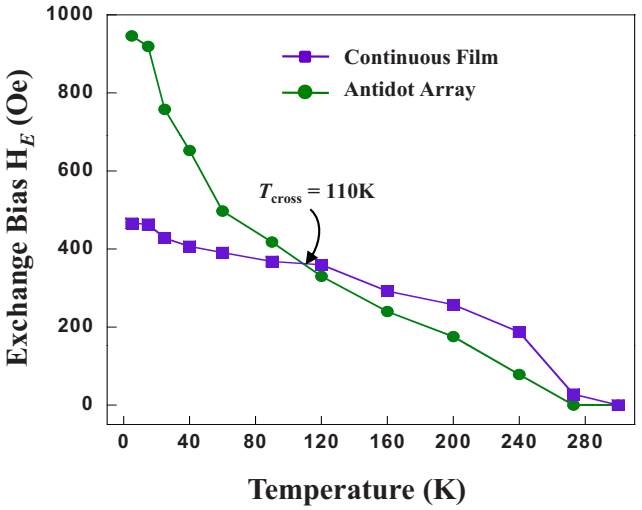

FIG. 3. (Color online) Dependence of exchange bias field H_E on temperature for both the Co (25 nm)/CoO (5 nm)/Cu (2 nm) antidot arrays and the corresponding continuous film.

results on the comparative magnitudes of H_E in nanostructured exchange biased systems and their continuous film counterparts. Figure 3 shows the dependence of H_E extracted from the AMR curves on temperature for the Co (25 nm)/CoO (5 nm)/Cu (2 nm) antidot arrays and the corresponding continuous film. We observed that H_E decreases with increasing temperature for both the antidot arrays and the continuous film. This decrease in H_E is attributed to the thermally induced weakening of the AFM pinning strength as temperature is increased. We also note that H_E decreases at a faster rate for the antidot arrays as compared to the continuous film for which the reduction in H_E is more gradual as temperature is increased. This may be ascribed to the fact that when compared to continuous films, AFM layers in nanostructures are more susceptible to thermal activation effects which results in the depinning of a large proportion of the AFM spin lattice.[13,14]

Recently, we have shown that due to the three-dimensional confinement of the AFM domains, the exchange bias fields in NiFe/IrMn antidot arrays are larger than the corresponding continuous films at room temperature.[12] The result is in agreement with Malozomoff's static model which predicts an inverse proportionality between the magnitude of H_E and AFM domain size.[50] Moreover, due to the presence of thicker AFM layers (t_{IrMn}=30 nm), thermal activation effects were negligible at room temperature for the NiFe/IrMn antidot arrays. In the present study, however, the thickness of the AFM layer is comparatively smaller (t_{CoO}=5 nm) and thus more prone to thermal activation. As a result, there is a strong competition between thermal activation effects which favor a reduction in H_E in nanostructures and constraints imposed on the AFM domain size by the reduced lateral dimensions of the antidot arrays, which favor an enhancement in H_E. Consequently, there is a crossover temperature T_{cross}=110 K in the evolution of H_E, which determines the temperature range in which H_E for the antidot arrays in either larger or smaller than the continuous film. It is evident that once thermal activation effects are minimized below 110 K, the antidot arrays exhibit larger exchange bias fields as compared to the continuous film.

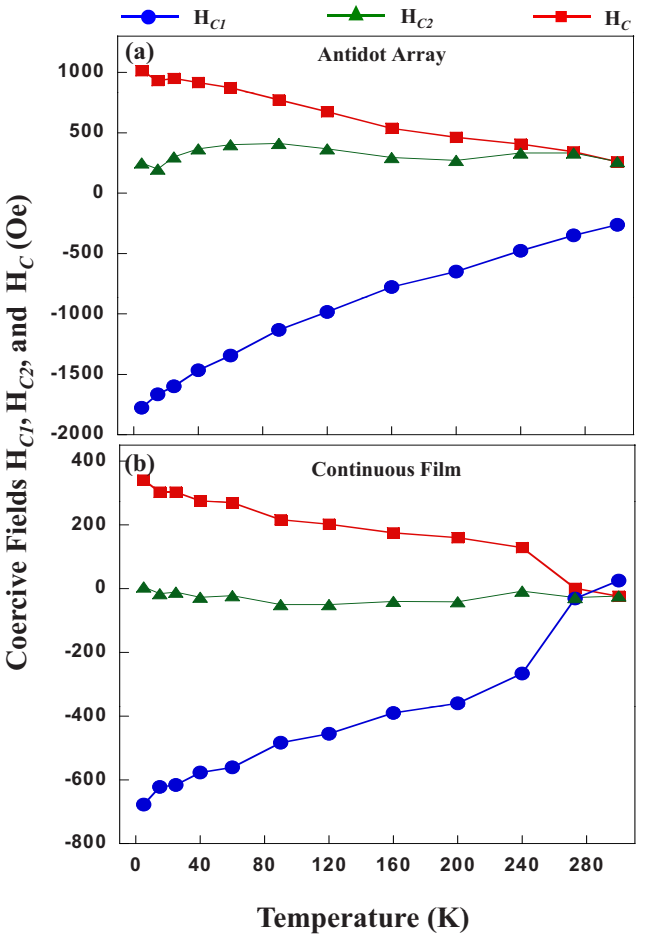

FIG. 4. (Color online) Temperature dependence of left coercive field H_{C1}, right coercive field H_{C2}, and overall coercive field H_C for Co (25 nm)/CoO (5 nm)/Cu (2 nm) (a) antidot arrays and (b) continuous film.

The temperature dependence of the coercive field was also investigated for the Co (25 nm)/CoO (5 nm)/Cu (2 nm) antidot arrays and the corresponding continuous film using AMR measurements. We define the coercive fields H_{C1} and H_{C2} as the fields at which the resistance is minimum in the decreasing and increasing branches of the AMR curves, respectively, and total coercive field $H_C=(H_{C2}-H_{C1})/2$. Figure 4 summarizes the analysis of temperature dependence of H_{C1}, H_{C2}, and H_C. We note a clear asymmetry in the temperature dependencies of H_{C1} and H_{C2}. For the antidot array, we observed that while the absolute value of H_{C1} increases monotonously with decreasing temperature, H_{C2} remains almost constant at ~350 Oe with varying temperatures, as shown in Fig. 4(a). For the continuous film similarly, Fig. 4(b) shows that H_{C2} remains fixed at −30 Oe while $|H_{C1}|$ increases as temperature is reduced. Consequently, the increase in H_C with decreasing temperature for the antidot arrays and the continuous film is primarily due to the increase in magnitude of H_{C1}. Although the temperature dependence of exchange bias field has been interpreted on the basis of theoretical models,[50–52] these models could not elucidate the

asymmetric temperature dependence of coercive fields H_{C1} and H_{C2}. To explain this phenomenon, Wang *et al.*,[53] considered the contribution of the AFM layer microstructure along with the exchange coupling between the FM and AFM layers. By taking into account the variation in spin arrangements at the FM-AFM interface, different temperature dependencies were obtained for H_{C1} and H_{C2}. Furthermore, it was also established that the temperature dependence of H_{C2} depends strongly on the factor $\kappa = A_{\mathrm{AFM0}}(A_{\mathrm{AFM0}}/K_{\mathrm{AFM0}})^{1/2}/(A_{\mathrm{FM}}d_{\mathrm{FM}})$, where A_{AFM0} and K_{AFM0} are the exchange stiffness and the anisotropy constant of the AFM layer at 0 K and A_{FM} and d_{FM} represent the exchange stiffness and thickness of the FM layer. For $\kappa < 1$, it was predicted that H_{C2} should remain effectively constant as temperature is varied from 300 to 5 K.[53] Our experimental results for the temperature dependence of coercive fields are in good qualitative agreement with this model, thereby suggesting that variations in spin orientations at the FM/AFM interface contribute to the coercive field in the decreasing branch (H_{C1}) of magnetization reversal but not during the increasing branch (H_{C2}). Using reasonable values from the literature for A_{AFM0}, K_{AFM0}, A_{FM},[1,54,55] and $d_{\mathrm{FM}}=25$ nm, we obtain $\kappa \ll 1$, and thus almost constant values for H_{C2} as temperature are varied.

C. Comparison of H_E obtained from AMR curves and hysteresis loops

To investigate the effects of measurement technique on the magnitude of exchange bias, the magnetic properties of the antidot arrays and the continuous film were also investigated using systematic hysteresis loop measurements. Figure 5 shows the representative hysteresis loops for Co (25 nm)/CoO (5 nm)/Cu (2 nm) antidot arrays and the corresponding continuous film as a function of temperature. The samples were field cooled in $H_{\mathrm{FC}}=5$ kOe from $T=300$ K (along the edge of the square lattice for the antidot array) and also measured along the same direction. The expected shift in the hysteresis loops, as well as the enhancement in coercive fields of the antidot arrays as compared to the continuous film due to pinning of domain walls in the vicinity of the antidots, is clearly discernible. We also observed that the exchange bias field H_E and the coercive fields extracted from the hysteresis loops do not coincide with those obtained from the AMR peak minima. To illustrate this scenario, we consider the hysteresis loops and the AMR curve for the antidot arrays at $T=90$ K. The coercive fields extracted from the decreasing and increasing branches of the hysteresis loops are −760 and 240 Oe, respectively, while the corresponding values obtained from the AMR peaks are −1780 and 220 Oe. Moreover, it was also observed that the magnitude of exchange bias field obtained from AMR measurements ($H_{E\text{-AMR}}=418$ Oe) exceeds the corresponding hysteresis loop shift ($H_{E\text{-Hys}}=261$ Oe). Similar discrepancies in the magnitudes of coercive and exchange bias fields obtained from the two measurements were also observed at other temperatures. This discrepancy may be attributed to the fact that AMR measurements determine the average pinning field across the entire FM-AFM interface, while in the case of hysteresis loops the exchange bias field is established by the weakest site for nucleation during the magnetization reversal process.[37] Hence, values of H_E determined from hysteresis loop shifts are significantly smaller than those obtained from AMR measurements and should be only considered as a lower limit to the actual magnitude of the exchange bias field. Our results are in good agreement with similar comparative studies of exchange bias fields obtained from hysteresis loops and AMR measurements.[37,38,56]

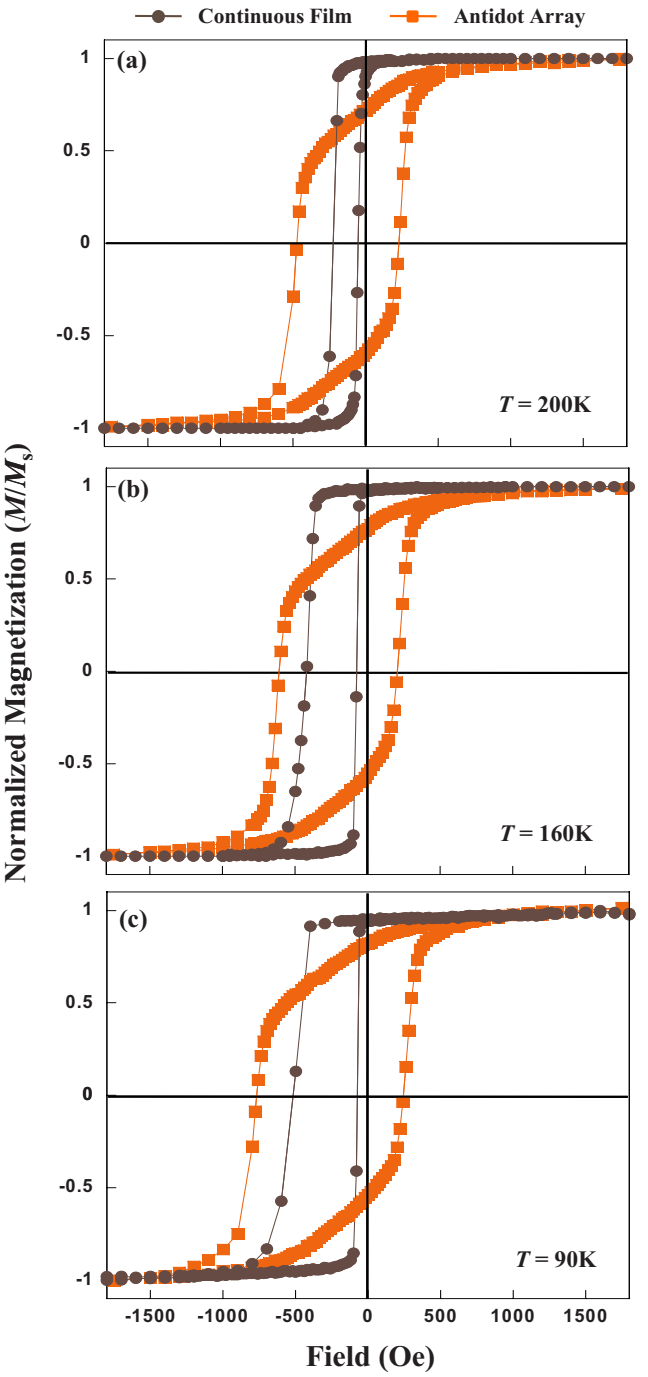

FIG. 5. (Color online) Normalized hysteresis curves for the exchange biased continuous film and antidot array of composition Co (25 nm)/CoO (5 nm)/Cu (2 nm) measured at (a) $T=200$ K, (b) $T=160$ K, and (c) $T=90$ K.

D. Effect of varying FM layer thickness

The exchange bias in the Co/CoO antidot arrays was further investigated by systematically varying the thickness of the Co layer t_{Co} from 25 to 100 nm while keeping other geometrical parameters and experimental conditions unchanged. Figure 6 shows the representative AMR curves for Co(t_{Co})/CoO(5 nm)/Cu(2 nm) antidot arrays corresponding to thicknesses t_{Co}=25, 50, 75, and 100 nm, respectively, and measured at T=5 K after exchange bias initialization using field-cooling techniques described in Sec. II. We observed that the magnetization reversal in the antidot arrays is strongly dependent on the Co layer thickness t_{Co} The evolution in the asymmetry of the AMR curves is evident as t_{Co} is increased from 25 nm to 100 nm. While the asymmetry in magnetization reversal is relatively small for t_{Co}=25 nm (~0.012%), it increases gradually with increasing t_{Co} and manifests itself clearly in the AMR curve shown in Fig. 6(d), corresponding to t_{Co}=100 nm. Quantitatively, we observed that the asymmetry in the AMR curves corresponding to the exchange biased antidot arrays has increased to 0.112% for t_{Co}=100 nm at T=5 K. As discussed earlier, the degree of asymmetry in the magnetization reversal is determined by the competition between FM uniaxial anisotropy and the interfacial FM-AFM exchange anisotropy.[44] This suggests that the asymmetry would increase for larger K_U, or weaker FM-AFM coupling. Indeed, as the thickness of the Co layer is increased, the interfacial FM-AFM coupling in the antidot arrays remains identical, while the effective FM anisotropy increases. As a result, the K_U/K_E ratio is larger for thicker Co layers, thus explaining the enhanced asymmetry in the AMR curves as t_{Co} is increased.

The evolution in the magnitude of the exchange bias field H_E was also investigated for the antidot arrays as a function of t_{Co} at varying temperatures. Figure 7 shows the dependence of H_E on $1/t_{Co}$ at T=5, 40, 90, 160, and 200 K, respectively. It was observed that H_E decreases with increasing t_{Co} at all temperatures and exhibits a linear dependence on $1/t_{Co}$. This $1/t_{Co}$ dependence of H_E highlights the primarily interfacial nature of the FM-AFM coupling in the antidot arrays and is in agreement with exchange bias fields predicted by Meiklejohn and Bean.[3] According to the random-field model,[50] domains in the AFM layer are separated by domain walls perpendicular to the FM-AFM interface in conjunction with the presence of roughness at the interfaces, which would otherwise be perfectly compensated. The exchange bias is a consequence of the energy difference between the different random domains. Accordingly, the exchange bias field H_E is given by[1]

$$H_E \approx 2z(A_{AFM}K_{AFM})^{1/2}/(\pi^2 M_{FM}t_{FM}), \quad (1)$$

where z is a number of order unity, A_{AFM} and K_{AFM} are the exchange stiffness and anisotropy constants of the AFM layer, and M_{FM} and t_{FM} are the saturation magnetization and thickness of the FM layer, respectively. As predicted by Eq. (1), the dependence of H_E on t_{Co} for the antidot arrays follows an inverse proportionality between exchange bias field and FM layer thickness.

We have further investigated the effects of varying t_{Co} on the exchange bias fields by plotting $H_E t_{Co}$ as a function of

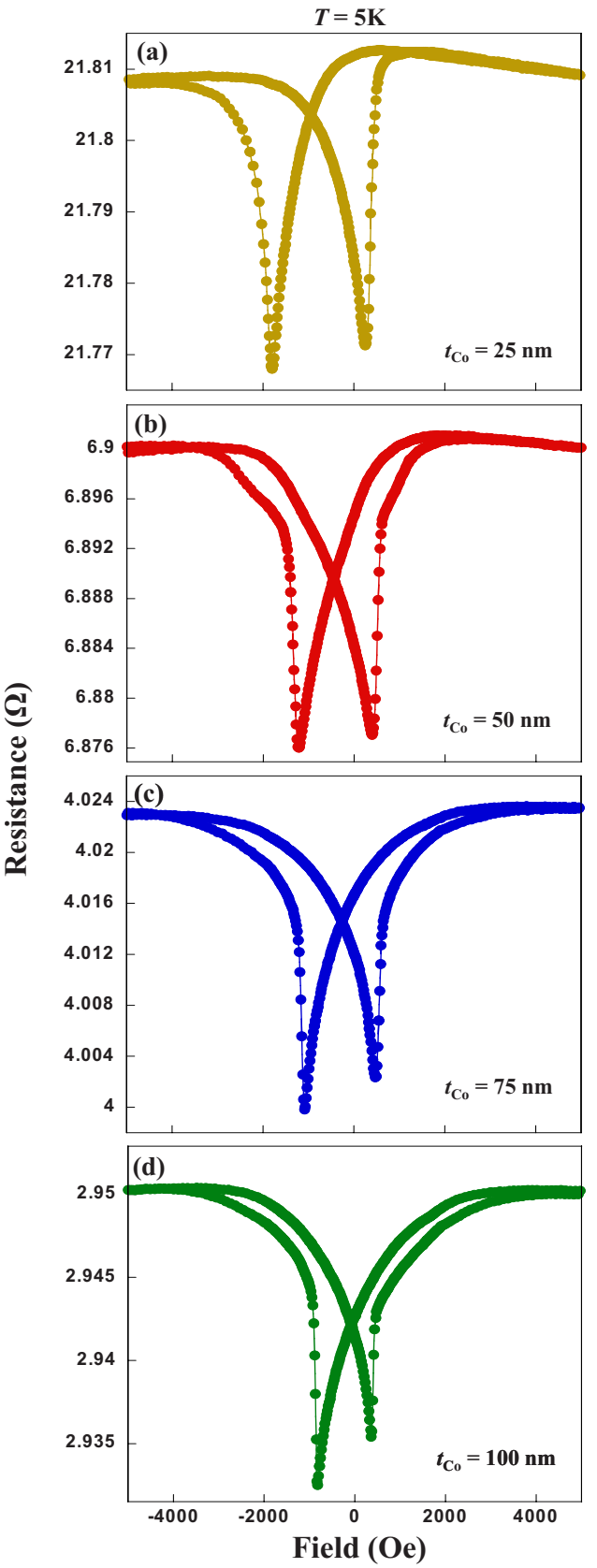

FIG. 6. (Color online) Longitudinal AMR curves for Co(t_{Co})/CoO(5 nm)/Cu(2 nm) antidot arrays at T=5 K corresponding to (a) t_{Co}=25 nm, (b) t_{Co}=50 nm, (c) t_{Co}=75 nm, and (d) t_{Co}=100 nm.

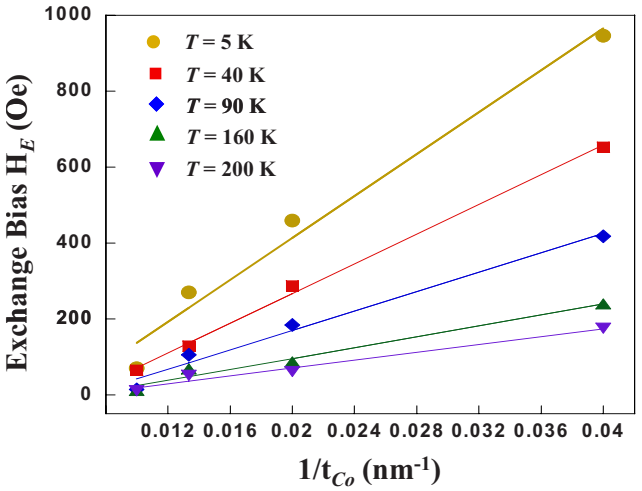

FIG. 7. (Color online) Dependence of exchange bias field H_E on the Co layer thickness t_{Co} for Co(t_{Co})/CoO(5 nm)/Cu(2 nm) antidot arrays as a function of temperature. The lines are $1/t_{\mathrm{Co}}$ linear fits of the H_E evolution at varying temperatures.

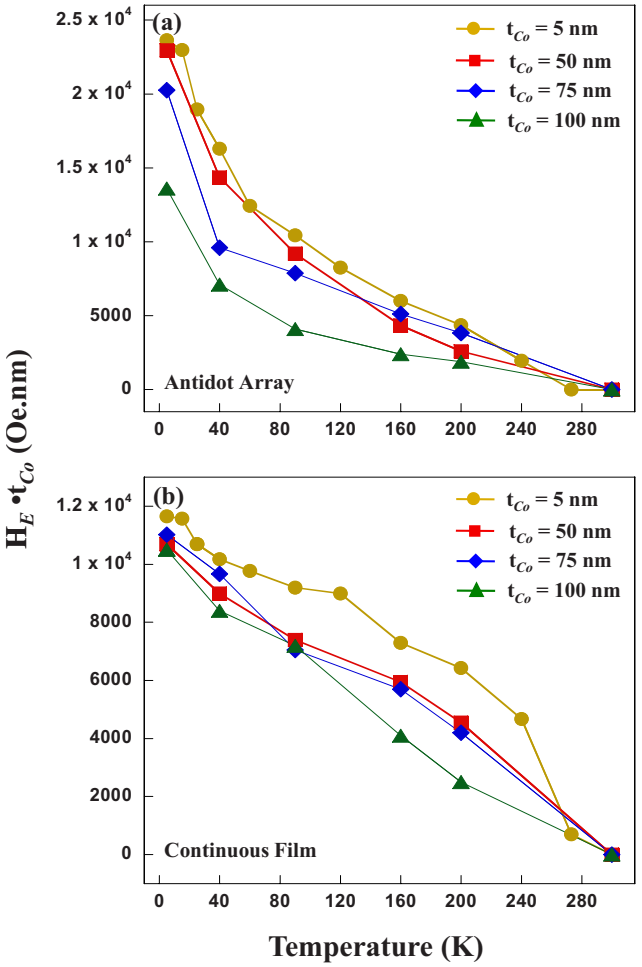

FIG. 8. (Color online) Temperature dependence of $H_E t_{\mathrm{Co}}$ corresponding to t_{Co}=25, 50, 75, and 100 nm, respectively, for (a) antidot array and (b) continuous film of composition Co(t_{Co})/CoO(5 nm)/Cu(2 nm).

temperature for the Co(t_{Co})/CoO(5 nm)/Cu(2 nm) antidot arrays and the corresponding continuous film. Figure 8 shows that our data do not exhibit a universal scaling of temperature and FM layer thickness with respect to H_E for both the antidot array and the continuous film. This is in contrast to a recent study by Polisetty *et al.*[57] on the scaling behavior of exchange bias where each individual data set follows an empirically linear temperature dependence and the entire data collapses on a virtually linear master curve. The temperature dependence of $H_E t_{\mathrm{Co}}$ was also used to determine the difference in blocking temperatures T_B for the antidot arrays and the continuous film. We observed that while T_B for the continuous film is close to the Néel temperature for bulk CoO, it is lower by ~18 K for the antidot arrays. This is attributed to the fact that thermal activation effects in the AFM layer are more pronounced in the antidot array as compared to the continuous film. Hence, the depinning of a large proportion of the AFM spin lattice in the antidot arrays results in a reduction in blocking temperature T_B for the antidot arrays.

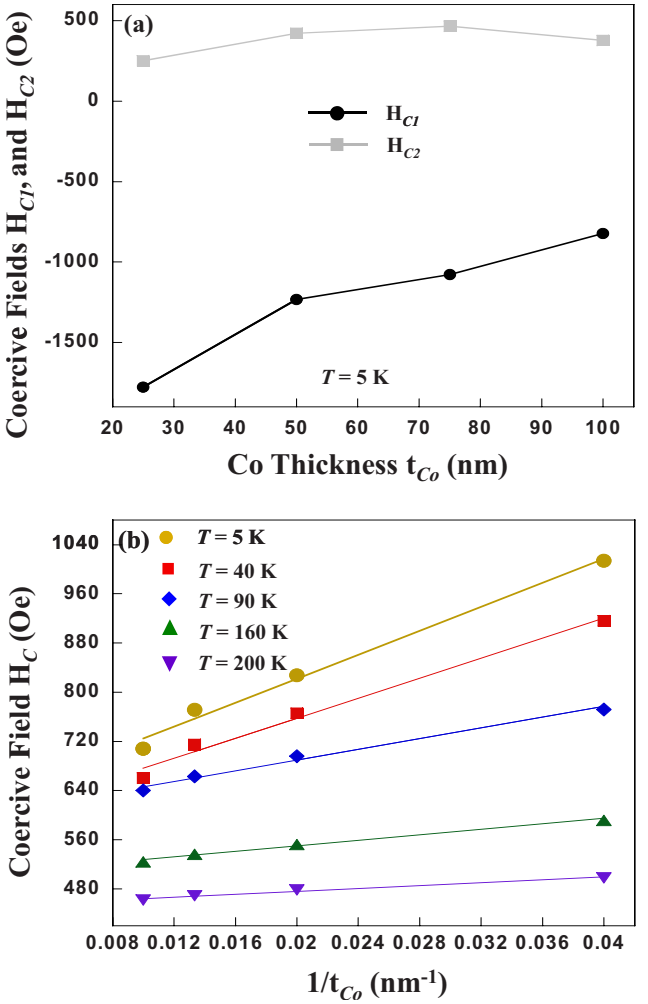

FIG. 9. (Color online) (a) Co layer thickness t_{Co} dependence of Co(t_{Co})/CoO(5 nm)/Cu(2 nm) antidot arrays for (a) left coercive field H_{C1}, right coercive field H_{C2} at T=5 K, and (b) overall coercive field H_C at varying temperatures. The lines are $1/t_{\mathrm{Co}}$ linear fits of the H_C evolution at different temperatures.

Figure 9 shows the variation in the coercive fields of the exchange biased antidot arrays as a function of t_{Co}. We observed that for any temperature below T_N, the right coercive field H_{C2} remains almost constant with varying t_{Co}, while the magnitude of the left coercive field H_{C1} decreases with increasing t_{Co}. This behavior is illustrated for $T=5$ K in Fig. 9(a), which clearly shows that the reduction in the overall coercive field H_C with increasing t_{Co} is primarily due to the decrease in H_{C1}. Similar dependencies for H_{C1} and H_{C2} were also observed at other temperatures. This unusual asymmetry may be understood on the basis of a model proposed by Tang *et al.*,[58] which extends the idea of Mauri *et al.*,[59] by incorporating higher-order anisotropy energy terms into the total free energy δ at the FM-AFM interface. By minimizing δ, it was ascertained that due to the presence of higher-order anisotropies in the exchange biased system, the right coercive field H_{C2} remains almost constant, while the left coercive field H_{C1} decreases substantially with increasing FM layer thickness. In Fig. 9(b), we present the dependence of coercive field H_C on $1/t_{Co}$ at varying temperatures. A consistent $1/t_{Co}$ linear dependence similar to H_E is clearly observed at all temperatures, indicative of the interfacial nature of the exchange bias in the antidot arrays. The linear dependence of H_C on inverse FM layer thickness is consistent with experimental observation in exchange biased systems.[4,58,60,61]

IV. CONCLUSIONS

In summary, we have investigated the exchange bias in Co/CoO nanoscale antidot arrays using systematic AMR measurements as a function of temperature and Co layer thickness t_{Co}. It was observed that while the continuous film exhibits asymmetry in the magnetization reversal due to different reversal mechanisms dominating the increasing and decreasing branches of the curve, the corresponding asymmetry in the antidot arrays is significantly smaller. This difference in asymmetry is ascribed to the configurational anisotropy in antidot arrays with square lattice geometry and competition between the FM uniaxial anisotropy and interfacial FM-AFM exchange anisotropy. The temperature dependence of exchange bias field H_E was also examined, and a strong competition between thermal activation effects and AFM domain size confinement imposed by the reduced lateral dimensions of the antidot arrays was observed. H_E for the antidot arrays was thus smaller or larger than the continuous film, depending on the temperature. Additionally, the temperature dependence of coercive fields demonstrated an asymmetric behavior in the left and right coercive fields with varying temperature, which could be understood by considering the variations in spin arrangements at the FM-AFM interface. The effect of varying the FM layer thickness in the antidot arrays was also studied, and it was demonstrated that due to increased FM anisotropy with increasing t_{Co}, the K_U/K_E ratio was larger for thicker Co layers, thus resulting in enhanced asymmetry in the AMR curves.

ACKNOWLEDGMENTS

This work was supported by the Agency of Science, Technology and Research (A*Star), Singapore under Grant No. 062-101-0022. The authors would like to thank N. Singh from Institute of Microelectronics (IME), Singapore for his assistance in template fabrication.

*Corresponding author; eleaao@nus.edu.sg

[1] A. E. Berkowitz and K. Takano, J. Magn. Magn. Mater. **200**, 552 (1999).
[2] M. Kiwi, J. Magn. Magn. Mater. **234**, 584 (2001).
[3] W. H. Meiklejohn and C. P. Bean, Phys. Rev. **105**, 904 (1957).
[4] J. Nogues and I. K. Schuller, J. Magn. Magn. Mater. **192**, 203 (1999).
[5] R. L. Stamps, J. Phys. D **33**, R247 (2000).
[6] C. Leighton, M. R. Fitzsimmons, A. Hoffmann, J. Dura, C. F. Majkrzak, M. S. Lund, and I. K. Schuller, Phys. Rev. B **65**, 064403 (2002).
[7] T. C. Schulthess and W. H. Butler, Phys. Rev. Lett. **81**, 4516 (1998).
[8] M. D. Stiles and R. D. McMichael, Phys. Rev. B **59**, 3722 (1999).
[9] J. C. S. Kools, IEEE Trans. Magn. **32**, 3165 (1996).
[10] A. O. Adeyeye and N. Singh, J. Phys. D **41**, 153001 (2008).
[11] J. I. Martin, J. Nogues, K. Liu, J. L. Vicent, and I. K. Schuller, J. Magn. Magn. Mater. **256**, 449 (2003).
[12] D. Tripathy, A. O. Adeyeye, and N. Singh, Appl. Phys. Lett. **93**, 022502 (2008).
[13] V. Baltz, J. Sort, B. Rodmacq, B. Dieny, and S. Landis, Phys. Rev. B **72**, 104419 (2005).
[14] M. Fraune, U. Rudiger, G. Guntherodt, S. Cardoso, and P. Freitas, Appl. Phys. Lett. **77**, 3815 (2000).
[15] J. Nogues, J. Sort, V. Langlais, V. Skumryev, S. Surinach, J. S. Munoz, and M. D. Baro, Phys. Rep. **422**, 65 (2005).
[16] K. Liu, S. M. Baker, M. Tuominen, T. P. Russell, and I. K. Schuller, Phys. Rev. B **63**, 060403(R) (2001).
[17] A. Nemoto, Y. Otani, S. G. Kim, K. Fukamichi, O. Kitakami, and Y. Shimada, Appl. Phys. Lett. **74**, 4026 (1999).
[18] V. Baltz, J. Sort, B. Rodmacq, B. Dieny, and S. Landis, Appl. Phys. Lett. **84**, 4923 (2004).
[19] E. Girgis, R. D. Portugal, H. Loosvelt, M. J. Van Bael, I. Gordon, M. Malfait, K. Temst, C. Van Haesendonck, L. H. A. Leunissen, and R. Jonckheere, Phys. Rev. Lett. **91**, 187202 (2003).
[20] J. Eisenmenger, Z.-P. Li, W. A. A. Macedo, and I. K. Schuller, Phys. Rev. Lett. **94**, 057203 (2005).
[21] Z.-P. Li, O. Petracic, J. Eisenmenger, and I. K. Schuller, Appl. Phys. Lett. **86**, 072501 (2005).
[22] A. Hoffmann, M. Grimsditch, J. E. Pearson, J. Nogués, W. A. A. Macedo, and I. K. Schuller, Phys. Rev. B **67**, 220406(R) (2003).
[23] V. Baltz, J. Sort, S. Landis, B. Rodmacq, and B. Dieny, Phys. Rev. Lett. **94**, 117201 (2005).
[24] G. Malinowski, M. Albrecht, I. L. Guhr, J. M. D. Coey, and S. van Dijken, Phys. Rev. B **75**, 012413 (2007).

[25] J. Sort, K. S. Buchanan, J. E. Pearson, A. Hoffmann, E. Menendez, G. Salazar-Alvarez, M. D. Baro, M. Miron, B. Rodmacq, B. Dieny, and J. Nogues, J. Appl. Phys. **103**, 07C109 (2008).
[26] M. S. Lund, W. A. A. Macedo, K. Liu, J. Nogués, I. K. Schuller, and C. Leighton, Phys. Rev. B **66**, 054422 (2002).
[27] A. N. Dobrynin, K. Temst, P. Lievens, J. Margueritat, J. Gonzalo, C. N. Afonso, E. Piscopiello, and G. V. Tendeloo, J. Appl. Phys. **101**, 113913 (2007).
[28] N. Singh, S. Goolaup, and A. O. Adeyeye, Nanotechnology **15**, 1539 (2004).
[29] R. H. Norton, IEEE Trans. Magn. **19**, 1579 (1983).
[30] C. C. Wang, A. O. Adeyeye, and Y. H. Wu, J. Appl. Phys. **97**, 10J902 (2005).
[31] C. C. Wang, A. O. Adeyeye, Y. H. Wu, and M. B. A. Jalil, J. Appl. Phys. **97**, 023521 (2005).
[32] C. C. Wang, A. O. Adeyeye, N. Singh, Y. S. Huang, and Y. H. Wu, Phys. Rev. B **72**, 174426 (2005).
[33] S. Brems, D. Buntinx, K. Temst, C. Van Haesendonck, F. Radu, and H. Zabel, Phys. Rev. Lett. **95**, 157202 (2005).
[34] B. H. Miller and E. D. Dahlberg, Appl. Phys. Lett. **69**, 3932 (1996).
[35] T. McGuire and R. Potter, IEEE Trans. Magn. **11**, 1018 (1975).
[36] M. Gierlings, M. J. Prandolini, H. Fritzsche, M. Gruyters, and D. Riegel, Phys. Rev. B **65**, 092407 (2002).
[37] T. Gredig, I. N. Krivorotov, and E. D. Dahlberg, J. Appl. Phys. **91**, 7760 (2002).
[38] T. Gredig, I. N. Krivorotov, and E. D. Dahlberg, Phys. Rev. B **74**, 094431 (2006).
[39] F. Radu, M. Etzkorn, R. Siebrecht, T. Schmitte, K. Westerholt, and H. Zabel, Phys. Rev. B **67**, 134409 (2003).
[40] K. Temst, E. Girgis, R. D. Portugal, H. Loosvelt, E. Popova, M. J. Van Bael, C. Van Haesendonck, H. Fritzsche, M. Gierlings, L. H. A. Leunissen, and R. Jonckheere, Eur. Phys. J. B **45**, 261 (2005).
[41] M. R. Fitzsimmons, P. Yashar, C. Leighton, I. K. Schuller, J. Nogués, C. F. Majkrzak, and J. A. Dura, Phys. Rev. Lett. **84**, 3986 (2000).
[42] P. Gogol, J. N. Chapman, M. F. Gillies, and F. W. M. Vanhelmont, J. Appl. Phys. **92**, 1458 (2002).
[43] J. McCord, R. Schafer, R. Mattheis, and K.-U. Barholz, J. Appl. Phys. **93**, 5491 (2003).
[44] J. Camarero, J. Sort, A. Hoffmann, J. M. Garcia-Martin, B. Dieny, R. Miranda, and J. Nogues, Phys. Rev. Lett. **95**, 057204 (2005).
[45] B. Beckmann, U. Nowak, and K. D. Usadel, Phys. Rev. Lett. **91**, 187201 (2003).
[46] A. N. Dobrynin, D. N. Ievlev, C. Hendrich, K. Temst, P. Lievens, U. Hormann, J. Verbeeck, G. Van Tendeloo, and A. Vantomme, Phys. Rev. B **73**, 245416 (2006).
[47] A. N. Dobrynin and R. Prozorov, J. Appl. Phys. **102**, 043902 (2007).
[48] K. Liu and C. L. Chien, IEEE Trans. Magn. **34**, 1021 (1998).
[49] C. C. Wang, A. O. Adeyeye, and N. Singh, Nanotechnology **17**, 1629 (2006).
[50] A. P. Malozemoff, Phys. Rev. B **35**, 3679 (1987).
[51] A. P. Malozemoff, Phys. Rev. B **37**, 7673 (1988).
[52] M. D. Stiles and R. D. McMichael, Phys. Rev. B **60**, 12950 (1999).
[53] J. Wang, W. N. Wang, X. Chen, H. W. Zhao, J. G. Zhao, and W. S. Zhan, Appl. Phys. Lett. **77**, 2731 (2000).
[54] J. van Lierop, B. W. Southern, K. W. Lin, Z. Y. Guo, C. L. Harland, R. A. Rosenberg, and J. W. Freeland, Phys. Rev. B **76**, 224432 (2007).
[55] O. Nakanishi and T. Yamada, J. Phys. Soc. Jpn. **36**, 1315 (1974).
[56] T. Gredig, I. N. Krivorotov, C. Merton, A. M. Goldman, and E. D. Dahlberg, J. Appl. Phys. **87**, 6418 (2000).
[57] S. Polisetty, S. Sahoo, and C. Binek, Phys. Rev. B **76**, 184423 (2007).
[58] Y. J. Tang, B. Roos, T. Mewes, S. O. Demokritov, B. Hillebrands, and Y. J. Wang, Appl. Phys. Lett. **75**, 707 (1999).
[59] D. Mauri, H. C. Siegmann, P. S. Bagus, and E. Kay, J. Appl. Phys. **62**, 3047 (1987).
[60] R. Jungblut, R. Coehoorn, M. T. Johnson, J. a. d. Stegge, and A. Reinders, J. Appl. Phys. **75**, 6659 (1994).
[61] C. Tsang, N. Heiman, and K. Lee, J. Appl. Phys. **52**, 2471 (1981).